Article

Natural and anthropogenic ethanol sources in North America and potential atmospheric impacts of ethanol fuel use

Dylan Millet, Eric Apel, Daven K. Henze, Jason Hill, Julian D Marshall, Hanwant Singh Singh, and Christopher Tessum

Environ. Sci. Technol., **Just Accepted Manuscript** • DOI: 10.1021/es300162u • Publication Date (Web): 25 Jun 2012

Natural and anthropogenic ethanol sources in North America and potential atmospheric impacts of ethanol fuel use

Dylan B. Millet[*1], *Eric Apel*[2], *Daven K. Henze*[3], *Jason Hill*[1], *Julian D. Marshall*[1], *Hanwant B. Singh*[4], *and Christopher W. Tessum*[1]

[1]University of Minnesota, Minneapolis-St. Paul, MN, USA.

[2]National Center for Atmospheric Research, Boulder, CO, USA.

[3]University of Colorado, Boulder, CO, USA.

[4]NASA Ames Resarch Center, Moffett Field, CA, USA.

* Corresponding author email: dbm@umn.edu

ABSTRACT: We use an ensemble of aircraft measurements with the GEOS-Chem chemical transport model to constrain present-day North American ethanol sources, and gauge potential long-range impacts of increased ethanol fuel use. We find that current ethanol emissions are underestimated by 50% in Western North America, and overestimated by a factor of two in the east. Our best estimate for year-2005 North American ethanol emissions is 670 GgC/y, with 440 GgC/y from the continental US. We apply these optimized source estimates to investigate two scenarios for increased ethanol fuel use in the US: one that assumes a complete transition from gasoline to E85 fuel, and one tied to the biofuel requirements of the US Energy Indepence and Security Act (EISA). For both scenarios, increased

ethanol emissions lead to higher atmospheric acetaldehyde concentrations (by up to 14% during winter for the All-E85 scenario) and an associated shift in reactive nitrogen partitioning reflected by an increase in the PAN:NO_y ratio. The largest relative impacts occur during fall, winter and spring because of large natural emissions of ethanol and other organic compounds during summer. Projected changes in atmospheric PAN reflect a balance between an increased supply of peroxyacetyl radicals from acetaldehyde oxidation, and the lower NO_x emissions for E85 relative to gasoline vehicles. The net effect is a general PAN increase in fall through spring, and a weak decrease over the US Southeast and the Atlantic Ocean during summer. Predicted NO_x concentrations decrease in surface air over North America (by as much 5% in the All-E85 scenario). Downwind of North America this effect is counteracted by higher NO_x export efficiency driven by increased PAN production and transport. From the point of view of NO_x export from North America, the increased PAN formation associated with E85 fuel use thus acts to offset the associated lower NO_x emissions.

1. INTRODUCTION

Ethanol (C_2H_5OH) is emitted to the atmosphere by vegetation, during biomass combustion, and as a result of various urban and industrial processes. It is also increasingly used in the US as a biofuel mixed with gasoline. In the atmosphere, ethanol is a precursor of acetaldehyde (CH_3CHO) and peroxyacetyl nitrate (PAN), so that changing ethanol emissions have the potential to affect urban air pollution and associated long-range transport. However, the significance of this effect will depend on the size of the emission change compared to that of the existing source fluxes, which are poorly known. Here we use a global 3D chemical transport model (GEOS-Chem CTM) applied to an ensemble of airborne observations to derive new constraints on natural and anthropogenic ethanol sources in North America. We then employ this revised source estimate as a baseline for assessing some potential large-scale impacts of changing ethanol fuel use in the US.

Biogenic emissions from terrestrial plants are thought to be the dominant global source of

atmospheric ethanol[1-3]. Ethanol is produced in plant tissues via fermentation reactions in leaves and roots[4-12]. It can then be oxidized to acetaldehyde and acetate and metabolized by the plant, but some of the ethanol (and acetaldehyde) is released to the atmosphere via leaf stomata[9]. There is also a smaller atmospheric ethanol source from dead and decaying plant matter[13-15].

Other ethanol sources are comparatively minor and include biomass combustion[16] and photochemical production via cross-reactions of peroxy radicals[17]. Anthropogenic sources include emissions from its use as a solvent, fuel, and chemical intermediate, as well as from fermentation and various industrial processes[18]. In previous work we estimated that natural emissions from living and decaying plants currently make up 90% of the global source of atmospheric ethanol[2].

Once in the atmosphere, photochemical oxidation by OH is the main ethanol sink, occurring on a timescale of ~4 days[19]. Ethanol is also soluble in water and can be removed by wet and dry deposition, which have been estimated to account for 23-35% of the total global sink[2,3]. Ethanol oxidation proceeds as:

$$CH_3CH_2OH + OH \rightarrow CH_3CH_2O + H_2O \quad (1a)$$

$$\rightarrow CH_3CHOH + H_2O \quad (1b)$$

$$\rightarrow CH_2CH_2OH + H_2O \quad (1c)$$

with reaction mainly (90%) via channel (1b). The alkoxy and α-hydroxyalkyl radicals produced from channels (1a) and (1b) go on to react with O_2 to produce acetaldehyde + HO_2[19,20], so that overall acetaldehyde is produced with ~95% yield. Acetaldehyde is classified as a hazardous air pollutant by the US EPA[21], and its subsequent oxidation can lead to production of ozone (O_3) and PAN, thus affecting the partitioning and fate of reactive nitrogen (NO_y). The β-hydroxyalkyl radical produced via channel (1c) predominantly goes on to produce glycoaldehyde and formaldehyde[20,22,23].

Ground-based ethanol measurements to constrain biogenic and anthropogenic sources are sparse, and as a result emission fluxes are uncertain. Aircraft measurements during the Intercontinental Transport Experiment, Phase A (INTEX-A, Jul-Aug 2004) and Phase B (INTEX-B, Apr-May 2006), and the Megacity Initiative: Local and Global Research Observations (MILAGRO, Mar 2006) featured extensive vertical profiling and boundary layer measurements over North America and the adjacent oceans. Our objective here is to apply these data to derive new information on North American ethanol emissions, and to use that information to evaluate some atmospheric impacts of potential future changes in ethanol fuel use, focusing on the role of ethanol as a precursor of acetaldehyde and PAN, and the associated effects on NO_y partitioning and export.

2. AIRCRAFT MEASUREMENTS

Figure 1 shows flight tracks for the aircraft campaigns used here. INTEX-A[24] took place during July-August 2004, with a focus on understanding tropospheric composition over North America, the outflow of pollution from North America, and its chemical evolution downwind. MILAGRO[25] and INTEX-B[26] were aimed at understanding air pollution transport from Mexico City and Asia and the associated climatic effects. MILAGRO was carried out over Mexico, the US Gulf Coast, and the Gulf of Mexico region during March 2006, while INTEX-B took place in April-May 2006 over the US West Coast and the Pacific Ocean. Details on the ethanol measurements for each campaign are provided in the Supporting Information (SI).

3. MODELING FRAMEWORK

We apply here the ethanol simulation implemented in GEOS-Chem by Millet et al.[2] GEOS-Chem (v8, http://www.geos-chem.org) is a global Eulerian chemical transport model driven by assimilated meteorological observations from the NASA Goddard Earth Observing System (GEOS-5.2.0[27]). The meteorological fields have 0.5°×0.667° horizontal resolution and 72 vertical layers. For our work here

we reduce the spatial resolution to 2°×2.5° and 47 layers, of which 14 are below 2 km altitude, and use a 15-minute transport timestep. We also use GEOS-4 data[28] to test the sensitivity of our results to the input meteorological data. Changes to the model physics, native horizontal and vertical resolution (1°×1.25° and 55 levels for GEOS-4), and observing system between GEOS-4 and GEOS-5 lead to significant differences in convection, boundary layer mixing, and wind speeds between the two datasets[29,30]. A detailed description of the GEOS-4 and GEOS-5 models, and the associated meteorological products, is provided elsewhere[27,28]. Simulations shown here are for 2006, and follow a 1-year model spinup.

Figure S1 shows North American ethanol sources as simulated by GEOS-Chem, and taken as a priori for our source optimization based on the aircraft observations. Biogenic ethanol emissions are computed online in GEOS-Chem using the Model of Emissions of Gases and Aerosols from Nature (MEGANv2.1)[2,31] as described in the SI. Fluxes are estimated for each model grid square as a sum of contributions from four plant functional types (PFTs - broadleaf trees, needleleaf trees, shrubs, and herbaceous plants [crops + grasses]), and the resulting North American fluxes are shown in Figure S1. Total contributions from broadleaf trees, needleleaf trees, and shrubs are similar (0.21-0.25 TgC/y), but each has a distinct spatial pattern reflecting that of the corresponding PFT. Predicted ethanol emissions from herbaceous plants (grasses and crops) are lower (0.06 TgC/y) and concentrated in the Central US. There have been only a few direct measurements of ethanol emissions from vegetation[10,14,32] and as a result the MEGANv2.1 flux estimates are quite uncertain, providing part of the motivation for this work.

A priori anthropogenic emissions over North America, including emissions from ethanol-fueled vehicles, are from the US EPA's National Emission Inventory (NEI) for 2005[33]. As shown in Figure S1, annual anthropogenic emissions for North America total 0.22 TgC/y in the model, or 30% of the simulated biogenic source. Other minor ethanol sources included in the model (but not plotted in Figure

S1) include biomass combustion and photochemical production (0.001 and 0.004 TgC/y, respectively over North America), calculated as in Millet et al.[2]

Photochemical destruction of ethanol by OH is computed in the model based on a rate constant[19] $k = 3.0\times10^{-12}\exp(20/T)$ applied to global OH fields archived from a full-chemistry GEOS-Chem simulation. Other ethanol sinks include wet and dry deposition. Modeled wet deposition in GEOS-Chem includes scavenging in wet convective updrafts, rainout and washout from convective anvils and large-scale precipitation[34,35], while dry deposition follows a resistance-in-series model[36,37]. Modeled photochemical and depositional sinks for ethanol are plotted in Figure S1 over North America, and together result in a global annual average lifetime of 3 days.

Figure S2 shows the sensitivity of the simulated ethanol concentrations along the aircraft flight tracks to the various North American ethanol sources described above. With the exceptions of photochemical production and biomass burning, we see from comparing Figures S2 and S1 that the combination of airborne datasets used here provides comprehensive coverage with respect to the distribution of North American source influences.

4. OPTIMIZED NORTH AMERICAN ETHANOL SOURCES

Figure 2 compares boundary layer (taken here as $P > 750$ hPa) ethanol measurements from the flight campaigns described in Section 2 to those simulated by GEOS-Chem along the flight track at the time of measurement. There are clear, and geographically specific, model biases. Most notably, simulated concentrations are too high in the Eastern US and too low in the Central and Western US. Here we apply these comparisons to derive the emission fluxes that are most consistent with the observational constraints using a Bayesian optimization approach.

Applying Bayes' theorem and assuming Gaussian error distributions, the optimal set of ethanol emissions is that which minimizes the cost function $J(\mathbf{x})$[38,39]:

$$J(\mathbf{x}) = (\mathbf{x} - \mathbf{x}_a)^T \mathbf{S}_a^{-1} (\mathbf{x} - \mathbf{x}_a) + (\mathbf{F}(\mathbf{x}) - \mathbf{y})^T \mathbf{S}_\Sigma^{-1} (\mathbf{F}(\mathbf{x}) - \mathbf{y}) \quad (3)$$

Here $\mathbf{y}$ is the vector of aircraft observations and $\mathbf{F}(\mathbf{x})$ the corresponding model values. The vector $\mathbf{x}$ represents the sources being optimized, with $\mathbf{x}_a$ their a priori (initial guess) values. $\mathbf{S}_a$ and $\mathbf{S}_\Sigma$ are the a priori and observational error covariance matrices. The minimum $J(\mathbf{x})$ thus defines the set of ethanol fluxes that minimizes the (error-weighted) mismatch between the aircraft data and the model, plus the (error-weighted) mismatch between the derived fluxes and their a priori values.

Previous work has shown that current models exhibit a severe low bias relative to ethanol measurements in remote areas and in the free troposphere[3]. Naik et al.[3] speculated that this might reflect a missing secondary source, or possibly measurement artifacts manifesting at very low ambient concentrations. We therefore focus our analysis on measurements over the North American continent and in the boundary layer (P > 750 hPa), in order to better isolate the signal from North American surface emissions. We also remove statistical outliers (> 0.95 quantile, representing 140 of 3792 datapoints) to avoid undue influence from fresh pollution plumes that are not resolved at the resolution of the CTM.

Our initial analyses employed a state vector composed of scale factors for specific emission categories: biogenic ethanol emissions from each of the four plant functional types, and anthropogenic emissions. However, optimizing the state vector in this way did not lead to a significant reduction in the cost function, perhaps indicating that the spatial distribution of fluxes within these categories is not accurately captured in the bottom-up estimates. We therefore optimize instead a state vector composed of four regional scale factors: ethanol emissions from the Western, Central, and Eastern parts of the US plus Canada, and from Mexico (Figure S3). Emission errors (estimated at 100%) for these four broad

regions can be assumed uncorrelated, so that $\mathbf{S}_a$ is diagonal. The observational error $\mathbf{S}_\Sigma$ includes both measurement and model error. The measurement uncertainty is estimated at 20% + 20 ppt (see SI). We further assume a 20% error in the forward model, representing the limit in the ability of the model to capture atmospheric gradients even if the emissions were perfectly correct. We apply these uncertainties independently to the measured and simulated concentrations, and add the results in quadrature to obtain the overall observing system error $\mathbf{S}_\Sigma$. Errors are assumed uncorrelated at the 2°×2.5° model resolution so that $\mathbf{S}_\Sigma$ is diagonal. Later we carry out a sensitivity analysis to assess the extent to which our findings depend on the specific construction of $\mathbf{S}_a$ and $\mathbf{S}_\Sigma$.

Table 1 shows the a posteriori correction factors for ethanol emissions from the four regions. We find a large model underestimate of ethanol emissions for the Western region, and a large overestimate for the Eastern region as well as for Mexico. Including all aircraft datasets as a single ensemble in the inversion, and solving for time-invariant scale factors, we infer a 53% model underestimate for the Western region and overestimates of a factor of 2 and 1.7 for the Eastern region and Mexico, respectively (a posteriori scale factors of 0.47 and 0.60). This west/east discrepancy is similar to recent findings for methanol based on satellite data[40]. There appears to be a persistent MEGAN underestimate of certain oxygenated volatile organic compound (VOC) emissions for plant types prevalent in the Western US compared to the Eastern US. Recent in-situ measurements in Central California imply very large methanol and ethanol emissions in that region (J. de Gouw, personal communication), apparently related to agriculture[41,42], and this is probably also a contributing factor. The base-case inversion indicates a 1.7× model overestimate for the Central US + Canada; however, based on the sensitivity analyses described below, emissions from this region are less well constrained by the aircraft observations.

Figure S4 compares the a posteriori boundary layer ethanol concentrations with the corresponding

aircraft observations. As we see, the high model bias in the Eastern US is removed, while the low bias in the Western US is reduced but not completely eliminated. As we discuss in the next section, this reflects the fact that the springtime, western-focused measurements indicate a larger correction to the modeled Western US source than do the summertime, eastern-focused measurements. The a posteriori simulation also shows evidence of a residual low bias in the North Central US; however, the sparse observational coverage over this region prevents any definitive constraint.

We thus estimate present-day ethanol emissions from the continental US at 440 GgC/year (Table 1). The corresponding emissions from North America as a whole are plotted in Fig. 3 (left column), and total 670 GgC/y with a strong seasonal cycle. This can be compared to the estimated present-day emissions for other non-methane VOCs, totaling 68 TgC/y (Figure S5, left column).

5. UNCERTAINTY ANALYSIS

Previous inverse analyses have shown that Bayesian a posteriori errors tend to underestimate the true uncertainty in the solution, and that a more accurate uncertainty estimate can be obtained by repeating the optimization while varying key forward model parameters and error specifications[43-46]. We follow that approach here, focusing on ethanol sinks and model transport as the two main model processes where inaccuracies could be conflated with an emission bias. Changing the specification of the a priori and observational error covariance matrices ($\mathbf{S}_a$ and $\mathbf{S}_\Sigma$) does not have a significant effect on the solution (< 1% change in the emission estimates for doubling or halving the error estimates).

Table 1 shows the results from an ensemble of sensitivity runs carried out to test the robustness of our optimization. Ethanol is removed from the atmosphere by reaction with OH and by deposition. Increasing the deposition efficiency for ethanol by allowing for reactive uptake by vegetation (increasing f_0 from 0 to 1)[47], or employing OH fields from a different model version (corresponding to a

6.4% decrease in global average OH), results in a ≤ 5% change to the inferred emissions from the Eastern US + Canada, Western US + Canada, and Mexico. Emissions from the Central US and Canada are slightly less well constrained, changing by 8-14% for these two sensitivity runs. All derived ethanol fluxes, particularly for the Central region, are more sensitive to the meteorological fields used to drive GEOS-Chem. Employing GEOS-4 rather than GEOS-5 meteorological data, with the associated changes to boundary layer mixing and ventilation[27-30], modifies our a posteriori emission estimates by +3%, -14%, and +17% for the Western region, Eastern region, and Mexico, respectively, and by +43% for the Central US + Canada. However, the a posteriori cost-function for the GEOS-4 based optimization is 40% higher than for GEOS-5, reflecting a much poorer ability to match the observations with the GEOS-4 dataset.

There is also a temporal aspect to consider in this analysis. The aircraft measurements in the Western US took place during springtime while those in the east took place during summer, so part of the east-west discrepancy could reflect a bias in the modeled seasonality of emissions. To test this, we repeated the analysis separately for the springtime and summertime data. Both seasonal ensembles agree in confirming a model underestimate of the Western US source. The correction indicated by the springtime, western-focused data alone (+79%) is significantly larger than implied by the summertime data alone (+35%). This may indicate a stronger biogenic source underestimate in the model earlier versus later in the growing season, as has been seen for methanol[48,49]. Another factor to consider is that the western-focused INTEX-B/MILAGRO data were collected in 2006, two years later than the eastern-focused INTEX-A data; increases in anthropogenic ethanol emissions between 2004-2006 thus may also contribute to the observed east-west discrepancy. When considered alone, the summer campaigns imply a 2× decrease in emissions from the Eastern US, nearly identical to the result using the full data ensemble. The springtime data alone do not have adequate sensitivity to constrain ethanol emissions from the Central or Eastern US (Figure S6), due to the western-focused flight strategy and prevailing

west-to-east winds.

For the time-invariant inversion, the a posteriori cost function is a factor of 1.5 lower than the a priori cost function (Table 1), indicating a significant reduction in model bias, but also some residual model error. This could partly reflect a seasonality bias as discussed above. Model errors related to the spatial distribution of ethanol emissions within each of the regions used to construct the state vector probably also contribute. More long-term observations are needed to resolve these issues, and to develop better constraints on seasonal ethanol emissions from different landscapes. Expanded measurements of the carbon isotopic signature of atmospheric ethanol would also help to better refine source estimates[50].

While the above sensitivity runs do not span every conceivable source of model and observational error, they do serve to assess some key sources of uncertainty and their relative magnitude. In particular, uncertainties associated with limited data coverage and model transport emerge as predominant error sources in constraining the present-day ethanol budget. Overall, our sensitivity analyses are all within 17% of our best-guess optimization for the Western, Eastern, and Mexican regions. Emissions from the Central part of the US and Canada are less well constrained (varying by up to 43% depending on the model configuration), since none of the flight campaigns focused on this area. However, the derived ethanol source for the continental US as a whole (440 GgC/y, Table 1) is highly consistent between the optimizations, varying by a maximum of 6% for the different inversions. Similarly, total North American emissions (estimated at 671 GgC/y) differ by at most 11% between the various sensitivity runs when using the full aircraft data ensemble.

6. POTENTIAL LARGE-SCALE EFFECTS OF INCREASED ETHANOL FUEL USE

In this section we use our new, top-down ethanol source estimates for North America as a baseline for examining some potential effects of increasing US ethanol fuel use. Previous work has explored how air

quality impacts of a transition to ethanol fuel might affect human health among the US population[51,52]. Here, we focus on potential larger-scale atmospheric impacts and air pollution transport, with an emphasis on the importance of ethanol as a precursor of acetaldehyde and PAN, and the related effects on NO_y partitioning and export.

We investigate two scenarios, and employ 2005 as our baseline year to match the NEI-2005 emission inventory. Total US gasoline consumption in 2005 was approximately 140 billion gallons (bg), compared to 4.0 bg of ethanol fuel[53]. The first scenario assumes a complete transition of US gasoline vehicles to E85 (85% ethanol, 15% gasoline) fuel. For this scenario, current gasoline vehicle emissions in the model are switched to the corresponding emission profiles for E85 vehicles. While today's vehicle fleet is not capable of running entirely on E85 fuel, we apply this scenario as a diagnostic to evaluate the potential for E85 fuel use to affect long-range atmospheric chemistry relative to a similar vehicle fleet running mainly on gasoline.

The second scenario reflects the US Energy Independence and Security Act (EISA) of 2007, requiring the use of 36 bg/y of biofuel by 2022. We examine here implications of meeting this requirement entirely with ethanol fuel. Because of the lower energy density of ethanol compared to gasoline, 36 bg of ethanol is approximately equivalent to 24 bg of gasoline[54]. To meet the EISA mandate in the model scenario, we assume all gasoline is blended with 10% ethanol, and then increase E85 use to the point where total US ethanol consumption reaches 36 billion gallons. Accounting for the use of denaturant, this results in consumption of 126 bg/y of E10 (at 97% the energy content of gasoline[54]) and 28 bg/y of E85 (at 71% the energy content of gasoline[54]). For both the All-E85 and EISA scenarios, we consider only changes to tailpipe emissions; our future work will quantify full life-cycle emission changes for various biofuel production strategies.

There is a marked shift in the speciation of emitted VOCs for ethanol-based fuel versus gasoline, with the dominant organic compound emitted by E85-fueled vehicles being ethanol itself[55]. VOC speciation profiles used here for E10 and E85 emissions are based on the EPA NEI-2005 recommendations. Changes in CO, NO_x, and total VOC emissions for E85 are computed based on the statistics compiled by Yanowitz and McCormick[55]. CO and NO_x emissions are reduced by 13% and 14% for E85 compared to gasoline, corresponding to the overall geometric mean difference between E85 vehicles and similar non-flex-fuel vehicles based on EPA certification data[55]. The corresponding change in total VOC emissions is not statistically significant, so we keep this unchanged between E85 and gasoline vehicles. For E10 emissions, reported measurements show a decrease in CO emissions compared to gasoline, with measured reductions between 12-25% for specific vehicles[56]. Fleet-wide, EPA's MOBILE6.2 model predicts an average CO decrease of 6.7-7.5% for E10. There is no consistent evidence for a general decrease or increase in NO_x or total VOC emissions for E10 vehicles compared to gasoline, with some studies reporting an increase and others a decrease[56]. Here we assume a 7.5% decrease in CO emissions for E10 relative to gasoline vehicles, with no change in NO_x or total VOC emissions.

Figures 3 and S5 show emissions of ethanol and other VOCs for present-day and projected for the All-E85 and EISA scenarios (annual emissions of ethanol, other VOCs, CO and NO_x are summarized in Table S1). North American ethanol emissions increase by 1040 GgC/y (2.6×) in the All-E85 scenario, and by 175 GgC/y (1.3×) in the EISA scenario. Emissions from the continental US increase by 3.4× and 1.4× for the two scenarios. The relative perturbation is weakest in summer because of large natural emissions of ethanol (and other VOCs). For instance, in the All-E85 scenario, wintertime North American ethanol emissions increase by 600%, with ethanol alone then making up 6.7% of the total continental VOC source at this time of year. For the same scenario during summer, ethanol emissions increase by 70%, and account for only 1.7% of the total seasonal VOC source (Fig. 3, S5).

Figures 4 and S7 show projected changes in atmospheric ethanol, acetaldehyde, PAN:NO_y ratio, PAN, and NO_x for the All-E85 and EISA scenarios, respectively, over and downwind of North America. In each case, we see the largest fractional change during winter. For example, acetaldehyde concentrations increase by as much as 14% during winter and by up to 5% during summer for the All-E85 scenario (but by only 2% and 1% for the EISA scenario). This acetaldehyde increase leads to a larger supply of peroxy acetyl ($CH_3C(O)OO$) radicals and in turn a shift in reactive nitrogen partitioning, with PAN making up a larger fraction of total NO_y (Figure 4, S7).

PAN concentration changes reflect a competition between the increased supply of peroxyacetyl radicals from ethanol oxidation and the decreased NO_x emissions for E85 relative to gasoline vehicles. The net effect in our simulations is a PAN increase of up to 6% in the All-E85 scenario (1% in the EISA scenario) during fall, winter and spring. During summer there is an ample existing supply of $CH_3C(O)OO$ and other peroxyacyl radicals from oxidation of biogenic VOCs, so that the additional ethanol source represents a smaller perturbation, and the NO_x effect becomes more important. In fact, over the Southeast US and downwind of North America we see a weak PAN decrease during summer, driven by the lower NO_x emissions (Figure 4).

Figure 4 shows, for the All-E85 scenario, a widespread decrease in surface NO_x (as much as 5%) over North America due to the lower NO_x emissions for E85 relative to gasoline vehicles. This is accompanied by a modest regional decrease in surface ozone (of order 1%). We can expect that a NO_x decrease will increase ozone within NO_x-saturated urban cores; however, our global-scale model can not fully resolve such effects. Downwind of the continent, the lower NO_x emissions are offset by increased NO_x export efficiency associated with enhanced PAN formation. Over the Atlantic Ocean, instead of a NO_x decrease, we instead see a minor increase of up to 2% outside of the summer season (Figure 4). Only during summer, when biogenic VOC oxidation provides a strong continental source of peroxyacyl

radicals, is there an overall (weak) NO_x decrease downwind over the Atlantic associated with E85 use. Thus from the point of view of the amount of NO_x exported from North America, the increased PAN formation associated with E85 fuel use acts to offset the lower NO_x emissions. These seasonal effects are notably weaker for the EISA scenario (Figure S7) because the PAN perturbation is smaller, and because NO_x emissions are unchanged in the model between E10 and gasoline.

In addition to the tailpipe emissions considered here, the overall atmospheric impacts of increased ethanol fuel use will depend on emission changes during the full life-cycle of fuel production and distribution. Depending on the feedstocks used for ethanol production, this may also include landcover shifts that lead to changes in biogenic emissions of ethanol and other VOCs. Our results here provide new constraints on present-day ethanol sources from North America, and on the potential for increasing ethanol emissions to mediate how changing NO_x emissions affect the composition of continental outflow.

ACKNOWLEDGMENT: This work was carried out in part using computing resources at the University of Minnesota Supercomputing Institute. We thank Alex Guenther for his helpful input.

SUPPORTING INFORMATION AVAILABLE: Additional material related to the airborne ethanol measurements, model sources of ethanol and other VOCs, the ethanol source optimization, and projected changes to atmospheric composition for the EISA scenario are provided in the Supporting Information. This material is available free of charge via http://pubs.acs.org/.

REFERENCES

(1) Kirstine, W.V.; Galbally, I.E. The global atmospheric budget of ethanol revisited. *Atmos. Chem. Phys.* **2012**, *12*, 545–555.

(2) Millet, D.B.; Guenther, A.; Siegel, D.A.; Nelson, N.B.; Singh, H.B.; de Gouw, J.A.; Warneke, C.; Williams, J.; Eerdekens, G.; Sinha, V.; Karl, T.; Flocke, F.; Apel, E.; Riemer, D.D.; Palmer, P.I.; Barkley, M. Global atmospheric budget of acetaldehyde: 3D model analysis and constraints from in-situ and satellite observations. *Atmos. Chem. Phys.* **2010**, *10*, 3405-3425.

(3) Naik, V.; Fiore, A.M.; Horowitz, L.W.; Singh, H.B.; Wiedinmyer, C.; Guenther, A.; de Gouw, J.A.; Millet, D.B.; Goldan, P.D.; Kuster, W.C.; Goldstein, A. Observational constraints on the global atmospheric budget of ethanol. *Atmos. Chem. Phys.* **2010**, *10*, 5361-5370.

(4) Cojocariu, C.; Kreuzwieser, J.; Rennenberg, H. Correlation of short-chained carbonyls emitted from Picea abies with physiological and environmental parameters. *New Phytol.* **2004**, *162*, 717-727.

(5) Jardine, K.; Harley, P.; Karl, T.; Guenther, A.; Lerdau, M.; Mak, J.E. Plant physiological and environmental controls over the exchange of acetaldehyde between forest canopies and the atmosphere. *Biogeosciences* **2008**, *5*, 1559-1572.

(6) Jardine, K.J. The Exchange of acetaldehyde between plants and the atmosphere: Stable carbon isotope and flux measurements. PhD thesis, Stony Brook University, Stony Brook, NY, available at http://dspace.sunyconnect.suny.edu/handle/1951/45198, 2008.

(7) Kimmerer, T.W.; Macdonald, R.C. Acetaldehyde and ethanol biosynthesis in leaves of plants. *Plant Physiol.* **1987**, *84*, 1204-1209.

(8) Kreuzwieser, J.; Scheerer, U.; Rennenberg, H. Metabolic origin of acetaldehyde emitted by poplar (Populus tremula x P-alba) trees. *J. Exp. Bot.* **1999**, *50*, 757-765.

(9) Kreuzwieser, J.; Schnitzler, J.P.; Steinbrecher, R. Biosynthesis of organic compounds emitted by

plants. *Plant Biol.* **1999**, *1*, 149-159.

(10) Schade, G.W.; Goldstein, A.H. Fluxes of oxygenated volatile organic compounds from a ponderosa pine plantation. *J. Geophys. Res.* **2001**, *106*, 3111-3123.

(11) Schade, G.W.; Goldstein, A.H. Plant physiological influences on the fluxes of oxygenated volatile organic compounds from ponderosa pine trees. *J. Geophys. Res.* **2002**, *4082*, 10.1029/2001JD000532.

(12) Winters, A.J.; Adams, M.A.; Bleby, T.M.; Rennenberg, H.; Steigner, D.; Steinbrecher, R.; Kreuzwieser, J. Emissions of isoprene, monoterpene and short-chained carbonyl compounds from Eucalyptus spp. in southern Australia. *Atmos. Environ.* **2009**, *43*, 3035-3043.

(13) Isidorov, V.A.; Vinogorova, V.T.; Rafalowski, K. HS-SPME analysis of volatile organic compounds of coniferous needle litter. *Atmos. Environ.* **2003**, *37*, 4645-4650.

(14) Kirstine, W.; Galbally, I.; Ye, Y.R.; Hooper, M. Emissions of volatile organic compounds (primarily oxygenated species) from pasture. *J. Geophys. Res.* **1998**, *103*, 10605-10619.

(15) Warneke, C.; Karl, T.; Judmaier, H.; Hansel, A.; Jordan, A.; Lindinger, W.; Crutzen, P.J. Acetone, methanol, and other partially oxidized volatile organic emissions from dead plant matter by abiological processes: Significance for atmospheric HO_x chemistry. *Global Biogeochem. Cy.* **1999**, *13*, 9-17.

(16) Andreae, M.O.; Merlet, P. Emission of trace gases and aerosols from biomass burning. *Global Biogeochem. Cy.* **2001**, *15*, 955-966.

(17) Villenave, E.; Lesclaux, R. Kinetics of the cross reactions of CH_3O_2 and $C_2H_5O_2$ radicals with selected peroxy radicals. *J. Phys. Chem.* **1996**, *100*, 14372-14382.

(18) Howard, P.H., *Handbook of Environmental Fate and Exposure Data for Organic Chemicals, Volume II - Solvents*. CRC Press: New York, 1990.

(19) Atkinson, R.; Baulch, D.L.; Cox, R.A.; Crowley, J.N.; Hampson, R.F.; Hynes, R.G.; Jenkin, M.E.; Rossi, M.J.; Troe, J. Evaluated kinetic and photochemical data for atmospheric chemistry: Volume II - gas phase reactions of organic species. *Atmos. Chem. Phys.* **2006**, *6*, 3625-4055.

(20) Atkinson, R. Atmospheric chemistry of VOCs and NO_x. *Atmos. Environ.* **2000**, *34*, 2063-2101.

(21) *Chemical summary for acetaldehyde*; EPA 749-F-94-003a; US Environmental Protection Agency: Washington, DC, 1994; http://www.epa.gov/chemfact/s_acetal.txt.

(22) Jenkin, M.E.; Saunders, S.M.; Pilling, M.J. The tropospheric degradation of volatile organic compounds: A protocol for mechanism development. *Atmos. Environ.* **1997**, *31*, 81-104.

(23) Saunders, S.M.; Jenkin, M.E.; Derwent, R.G.; Pilling, M.J. Protocol for the development of the Master Chemical Mechanism, MCM v3 (Part A): Tropospheric degradation of non-aromatic volatile organic compounds. *Atmos. Chem. Phys.* **2003**, *3*, 161-180.

(24) Singh, H.B.; Brune, W.H.; Crawford, J.H.; Jacob, D.J.; Russell, P.B. Overview of the summer 2004 intercontinental chemical transport experiment - North America (INTEX-A). *J. Geophys. Res.* **2006**, *111*, D24S01, doi:10.1029/2006JD007905.

(25) Molina, L.T.; Madronich, S.; Gaffney, J.S.; Apel, E.; de Foy, B.; Fast, J.; Ferrare, R.; Herndon, S.; Jimenez, J.L.; Lamb, B.; Osornio-Vargas, A.R.; Russell, P.; Schauer, J.J.; Stevens, P.S.; Volkamer, R.; Zavala, M. An overview of the MILAGRO 2006 Campaign: Mexico City emissions and their transport and transformation. *Atmos. Chem. Phys.* **2010**, *10*, 8697-8760.

(26) Singh, H.B.; Brune, W.H.; Crawford, J.H.; Flocke, F.; Jacob, D.J. Chemistry and transport of pollution over the Gulf of Mexico and the Pacific: Spring 2006 INTEX-B campaign overview and first

results. *Atmos. Chem. Phys.* **2009**, *9*, 2301-2318.

(27) *The GEOS-5 Data Assimilation System - Documentation of Versions 5.0.1, 5.1.0, and 5.2.0*; NASA Global Modeling and Assimilation Office: Greenbelt, MD, 2008; http://gmao.gsfc.nasa.gov/pubs/docs/Rienecker369.pdf.

(28) *Documentation and Validation of the Goddard Earth Observing System (GEOS) Data Assimilation System - Version 4*; NASA Global Modeling and Assimilation Office: Greenbelt, MD, 2005; http://gmao.gsfc.nasa.gov/systems/geos4/Bloom.pdf.

(29) Jaeglé, L.; Quinn, P.K.; Bates, T.S.; Alexander, B.; Lin, J.T. Global distribution of sea salt aerosols: New constraints from in situ and remote sensing observations. *Atmos. Chem. Phys.* **2011**, *11*, 3137-3157.

(30) Liu, J.; Logan, J.A.; Jones, D.B.A.; Livesey, N.J.; Megretskaia, I.; Carouge, C.; Nedelec, P. Analysis of CO in the tropical troposphere using Aura satellite data and the GEOS-Chem model: Insights into transport characteristics of the GEOS meteorological products. *Atmos. Chem. Phys.* **2010**, *10*, 12207–12232.

(31) Guenther, A.; Karl, T.; Harley, P.; Wiedinmyer, C.; Palmer, P.I.; Geron, C. Estimates of global terrestrial isoprene emissions using MEGAN (Model of Emissions of Gases and Aerosols from Nature). *Atmos. Chem. Phys.* **2006**, *6*, 3181-3210.

(32) Fukui, Y.; Doskey, P.V. Air-surface exchange of nonmethane organic compounds at a grassland site: Seasonal variations and stressed emissions. *J. Geophys. Res.* **1998**, *103*, 13153-13168.

(33) EPA NEI 2005 inventory; http://www.epa.gov/oar/data/.

(34) Liu, H.Y.; Jacob, D.J.; Bey, I.; Yantosca, R.M. Constraints from Pb-210 and Be-7 on wet deposition and transport in a global three-dimensional chemical tracer model driven by assimilated

meteorological fields. *J. Geophys. Res.* **2001**, *106*, 12109-12128.

(35) Mari, C.; Jacob, D.J.; Bechtold, P. Transport and scavenging of soluble gases in a deep convective cloud. *J. Geophys. Res.* **2000**, *105*, 22255-22267.

(36) Wang, Y.H.; Jacob, D.J.; Logan, J.A. Global simulation of tropospheric O_3-NO_x-hydrocarbon chemistry: 1. Model formulation. *J. Geophys. Res.* **1998**, *103*, 10713-10725.

(37) Wesely, M.L. Parameterization of surface resistances to gaseous dry deposition in regional-scale numerical models. *Atmos. Environ.* **1989**, *23*, 1293-1304.

(38) Rodgers, C.D., *Inverse methods for atmospheric sounding: Theory and practice*. World Scientific: Singapore, 2000.

(39) Tarantola, A., *Inverse Problem Theory: Methods for Data Fitting and Model Parameter Estimation*. Elsevier: New York, 1987.

(40) Stavrakou, T.; Guenther, A.; Razavi, A.; Clarisse, L.; Clerbaux, C.; Coheur, P.F.; Hurtmans, D.; Karagulian, F.; De Mazière, M.; Vigouroux, C.; Amelynck, C.; Schoon, N.; Laffineur, Q.; Heinesch, B.; Aubinet, M.; Rinsland, C.; Müller, J.F. First space-based derivation of the global atmospheric methanol emission fluxes. *Atmos. Chem. Phys.* **2011**, *11*, 4873-4898.

(41) Hafner, S.D.; Montes, F.; Rotz, C.A.; Mitloehner, F. Ethanol emission from loose corn silage and exposed silage particles. *Atmos. Environ. 44*, 4172-4180.

(42) Malkina, I.L.; Kumar, A.; Green, P.G.; Mitloehner, F.M. Identification and Quantitation of Volatile Organic Compounds Emitted from Dairy Silages and Other Feedstuffs. *Journal of Environmental Quality 40*, 28-36.

(43) Arellano, A.F.; Hess, P.G. Sensitivity of top-down estimates of CO sources to GCTM transport.

Geophys. Res. Lett. **2006**, *33*, L21807, doi:10.1029/2006GL027371.

(44) Heald, C.L.; Jacob, D.J.; Jones, D.B.A.; Palmer, P.I.; Logan, J.A.; Streets, D.G.; Sachse, G.W.; Gille, J.C.; Hoffman, R.N.; Nehrkorn, T. Comparative inverse analysis of satellite (MOPITT) and aircraft (TRACE-P) observations to estimate Asian sources of carbon monoxide. *J. Geophys. Res.* **2004**, *109*, D23306, doi:10.1029/2004JD005185.

(45) Kopacz, M.; Jacob, D.; Henze, D.K.; Heald, C.L.; Streets, D.G.; Zhang, Q. A comparison of analytical and adjoint Bayesian inversion methods for constraining Asian sources of CO using satellite (MOPITT) measurements of CO columns. *J. Geophys. Res.* **2009**, *114*, D04305, doi:10.1029/2007JD009264.

(46) Peylin, P.; Baker, D.; Sarmiento, J.; Ciais, P.; Bousquet, P. Influence of transport uncertainty on annual mean and seasonal inversions of atmospheric CO_2 data. *J. Geophys. Res.* **2002**, *107*, 4385, doi:10.1029/2001JD000857.

(47) Karl, T.; Harley, P.; Emmons, L.; Thornton, B.; Guenther, A.; Basu, C.; Turnipseed, A.; Jardine, K. Efficient atmospheric cleansing of oxidized organic trace gases by vegetation. *Science* **2010**, *330*, 816-819.

(48) Hu, L.; Millet, D.B.; Mohr, M.J.; Wells, K.C.; Griffis, T.J.; Helmig, D. Sources and seasonality of atmospheric methanol based on tall tower measurements in the US Upper Midwest. *Atmos. Chem. Phys.* **2011**, *11*, 11145-11156.

(49) Wells, K.C.; Millet, D.B.; Hu, L.; Cady-Pereira, K.E.; Xiao, Y.; Shephard, M.W.; Clerbaux, C.L.; Clarisse, L.; Coheur, P.-F.; Apel, E.C.; Gouw, J.d.; Warneke, C.; Singh, H.B.; Goldstein, A.H.; Sive, B.C. Tropospheric methanol observations from space: Retrieval evaluation and constraints on the seasonality of biogenic emissions. *Atmos. Chem. Phys.* **2011**, *submitted*.

(50) Giebel, B.M.; Swart, P.K.; Riemer, D.D. New insights to the use of ethanol in automotive fuels: A stable isotopic tracer for fossil- and bio-fuel combustion inputs to the atmosphere. *Environ. Sci. Technol.* **2011**, *45*, 6661-6669.

(51) Hill, J.; Polasky, S.; Nelson, E.; Tilman, D.; Huo, H.; Ludwig, L.; Neumann, J.; Zheng, H.C.; Bonta, D. Climate change and health costs of air emissions from biofuels and gasoline. *P. Natl. Acad. Sci. USA* **2009**, *106*, 2077-2082.

(52) Jacobson, M.Z. Effects of ethanol (E85) versus gasoline vehicles on cancer and mortality in the United States. *Environ. Sci. Technol.* **2007**, *41*, 4150-4157.

(53) US Energy Information Administration; http://www.eia.gov/.

(54) US Department of Energy Transportation Energy Data Book; http://cta.ornl.gov/data/appendix_b.shtml.

(55) Yanowitz, J.; McCormick, R.L. Effect of E85 on tailpipe emissions from light-duty vehicles. *J. Air & Waste Manage. Assoc.* **2009**, *59*, 172-182.

(56) *Regulatory Impact Analysis: Renewable Fuel Standard Program*; EPA420-R-07-004; US Environmental Protection Agency (EPA): Washington, DC, 2007; http://www.epa.gov/otaq/renewablefuels/420r07004-sections.htm.

Table 1. North American ethanol sources: A priori forward model emissions versus a posteriori emissions optimized on the basis of aircraft measurements.

Simulation	Optimized Regions[1]				US Total[2]	North American Total	Cost Function Reduction
	Western Region	Central Region	Eastern Region	Mexico			
Ethanol Emissions (GgC/y)							
A Priori	148	243	370	208	613	969	-
Opt1[3]	227	146	174	124	440	671	1.52
Sensitivity Runs: Deviation From Best Guess Optimization Opt1							
Opt2-DEP[4]	+4%	+8%	+4%	+4%	+5%	+5%	1.44
Opt3-OH[5]	-3%	+14%	+5%	-5%	+4%	+2%	1.47
Opt4-MET[6]	+6%	+43%	-13%	+17%	+6%	+11%	1.42
Opt5-SPR[7]	+17%	NA	NA	-5%	NA	NA	1.66
Opt6-SUM[8]	-12%	-6%	+1%	NA	-6%	-17%	1.58

[1]Regions are defined as shown in Fig. S3. The Western, Central and Eastern regions include the US and Canada. [2]Continental US. [3]Best-guess optimization. [4]Optimization using increased dry deposition loss rate. [5]Optimization using modified OH concentrations (see text). [6]Optimization using GEOS-4 meteorological fields. [7]Optimization using springtime aircraft data only. [8]Optimization using summertime aircraft data only.

Figure 1. Airborne ethanol observations. Shown are flight tracks from the Intercontinental Transport Experiment, Phase A (INTEX-A: DC8 aircraft, Jul–Aug 2004) and Phase B (INTEX-B: DC8 and C130 aircraft, Apr-May 2006); and the Megacity Initiative: Local And Global Research Observations (MILAGRO: DC8 and C130 aircraft, Mar 2006). Flight tracks are plotted over boundary layer ethanol concentrations (P > 750 hPa, Mar-Aug mean) from the GEOS-Chem a priori simulation.

Figure 2. Difference plot showing ethanol concentrations in the boundary layer from the GEOS-Chem a priori simulation minus the corresponding measured values from the aircraft campaigns. Model values are sampled along the flight track at the time of the observations.

Figure 3. Seasonal ethanol emissions from North America. Emissions for present-day (based on the Opt1 source optimization) are compared to those for the EISA and All-E85 scenarios as described in the text. Numbers inset give the total North American ethanol source (Canada + US + Mexico).

Figure 4. Projected change (%) in atmospheric ethanol, acetaldehyde, PAN:NO_y ratio, PAN, and NO_x over and downwind of North America for a US transition to ethanol-based fuel (All-E85 scenario). The largest relative increases for ethanol, acetaldehyde and PAN occur during fall, winter and spring because of substantial biogenic emissions of ethanol and other VOCs during summer. NO_x emissions are lower for E85-fueled vehicles, but the associated concentration decrease downwind of North America is offset by increased long-range transport of PAN.

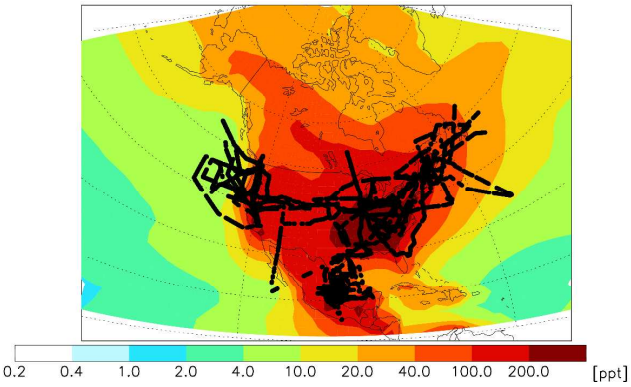

Figure 1. Airborne ethanol observations. Shown are flight tracks from the Intercontinental Transport Experiment, Phase A (INTEX-A: DC8 aircraft, Jul–Aug 2004) and Phase B (INTEX-B: DC8 and C130 aircraft, Apr-May 2006); and the Megacity Initiative: Local And Global Research Observations (MILAGRO: DC8 and C130 aircraft, Mar 2006). Flight tracks are plotted over boundary layer ethanol concentrations ($P > 750$ hPa, Mar-Aug mean) from the GEOS-Chem a priori simulation.

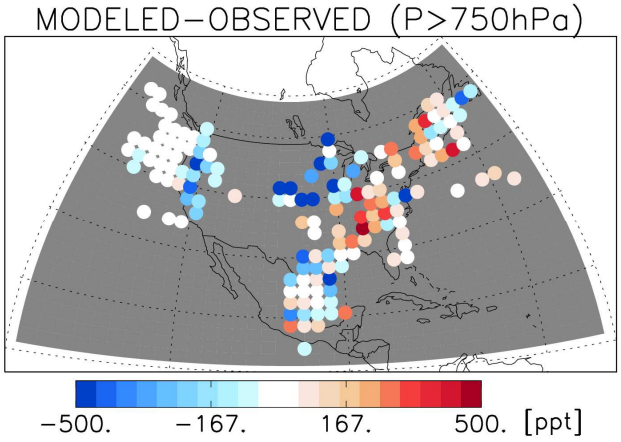

Figure 2. Difference plot showing ethanol concentrations in the boundary layer from the GEOS-Chem a priori simulation minus the corresponding measured values from the aircraft campaigns. Model values are sampled along the flight track at the time of the observations.

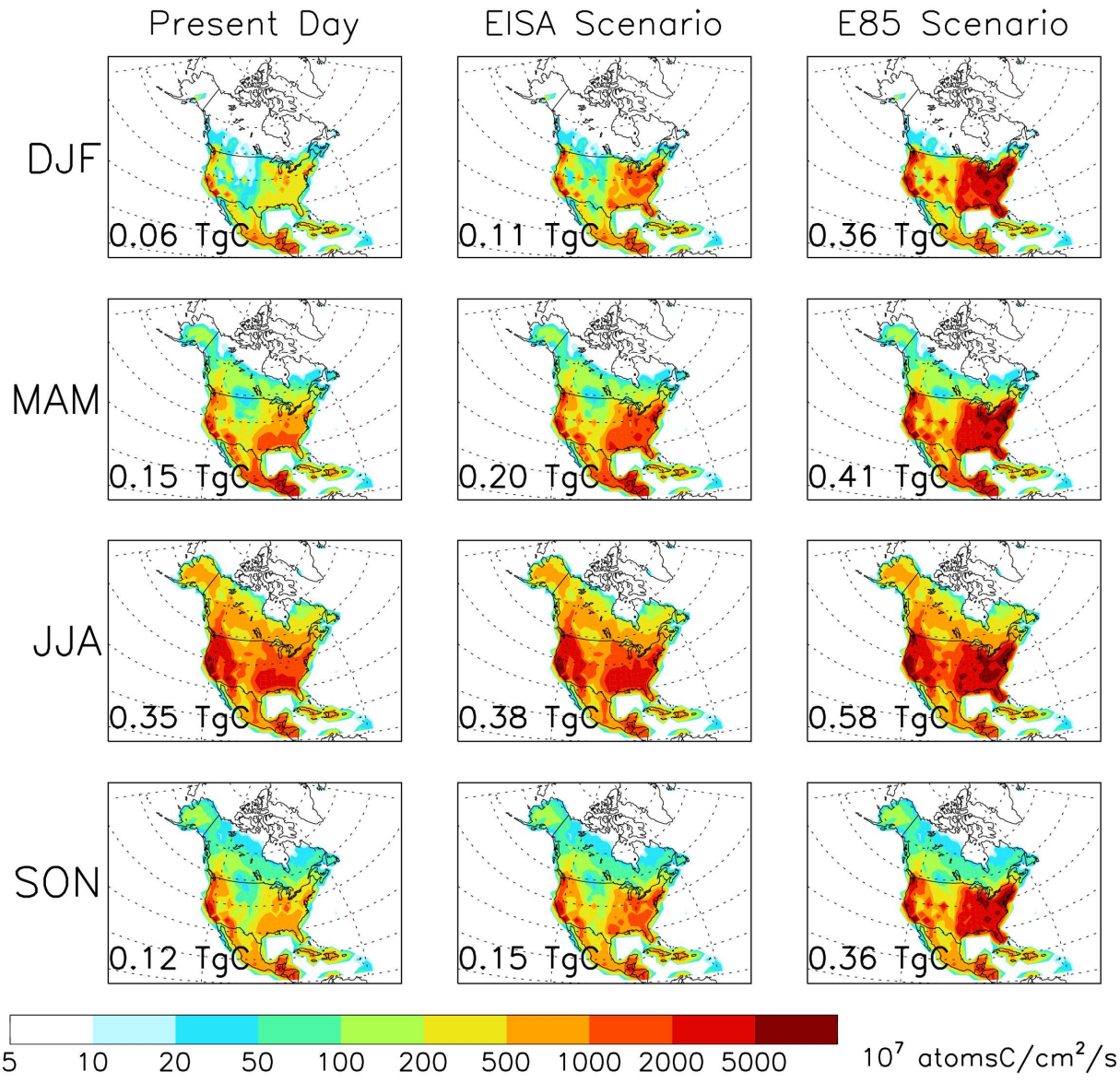

Figure 3. Seasonal ethanol emissions from North America. Emissions for present-day (based on the Opt1 source optimization) are compared to those for the EISA and All-E85 scenarios as described in the text. Numbers inset give the total North American ethanol source (Canada + US + Mexico).

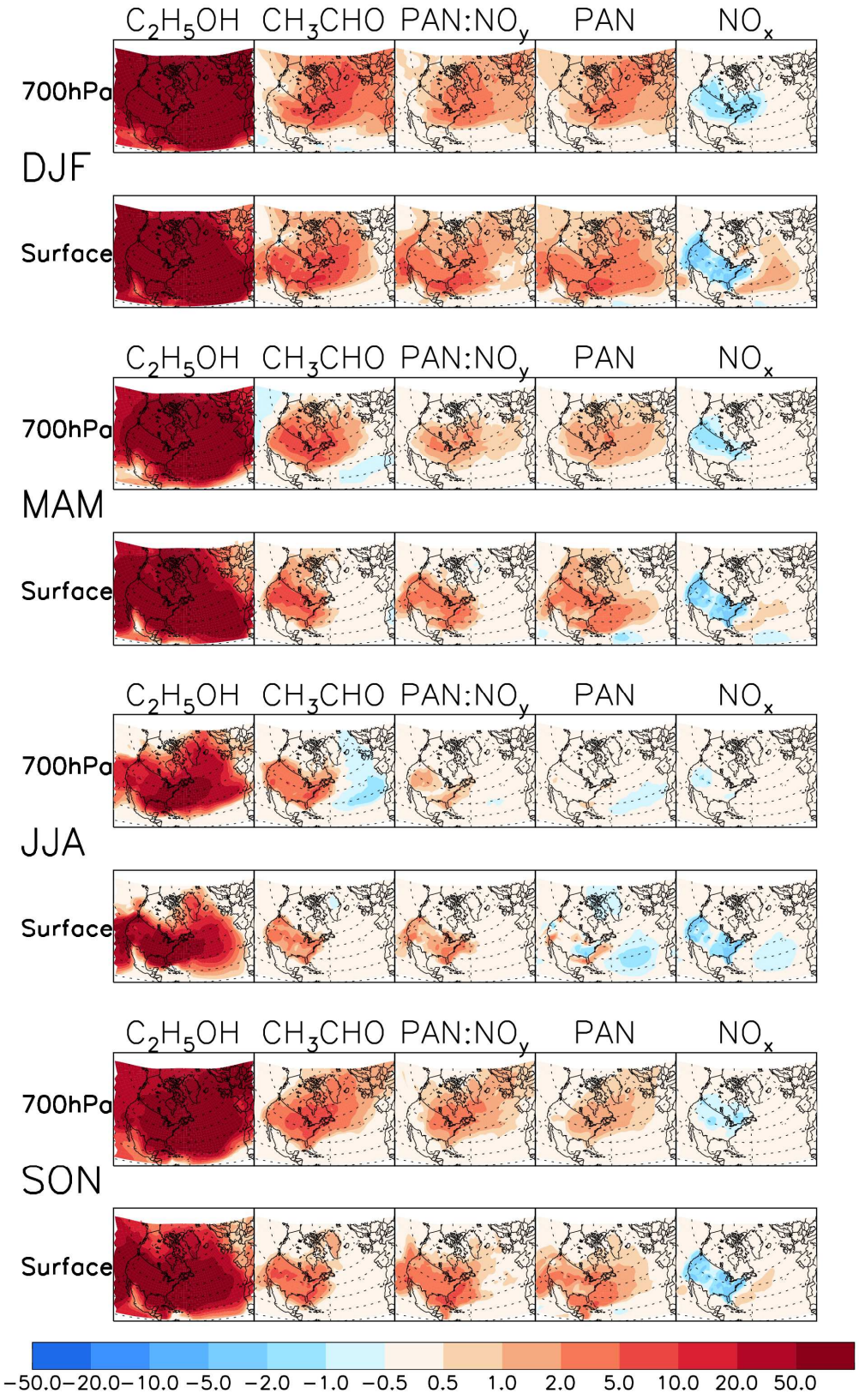

Figure 4. Projected change (%) in atmospheric ethanol, acetaldehyde, PAN:NO_y ratio, PAN, and NO_x

over and downwind of North America for a US transition to ethanol-based fuel (All-E85 scenario). The largest relative increases for ethanol, acetaldehyde and PAN occur during fall, winter and spring because of substantial biogenic emissions of ethanol and other VOCs during summer. NO_x emissions are lower for E85-fueled vehicles, but the associated concentration decrease downwind of North America is offset by increased long-range transport of PAN.

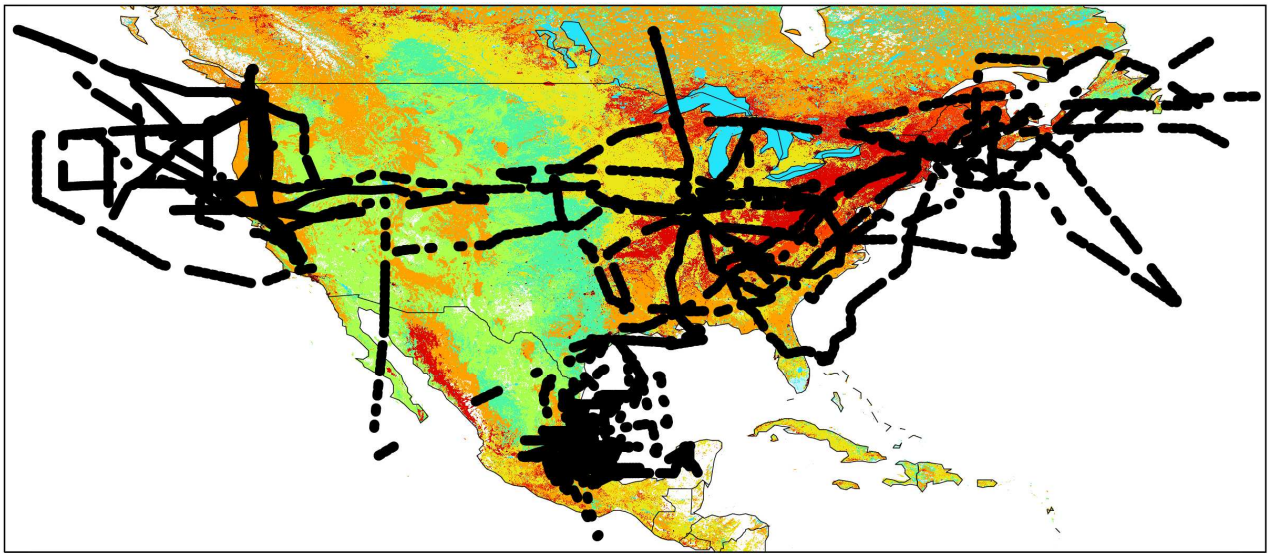

TOC Art.